Opportunities of copper addition in $CH_3NH_3PbI_3$ perovskite and their photovoltaic performance evaluation

Maria Khalid,*¶ Anurag Roy,¶ Shubhranshu Bhandari, Prabhakaran Selvaraj, Senthilarasu Sundaram and Tapas K. Mallick*

Environment and Sustainability Institute, University of Exeter, Penryn Campus, Cornwall TR10 9FE, U.K.

¶ Authors contributed equally

A B S T R A C T

Perovskite solar cells (PSCs) have encountered a fulgurant development in their power-conversion efficiency (PCEs) generation in the drive to provide a facile, cheap and clean source of energy over just a few years. The most efficient PSCs are fabricated using $CH_3NH_3PbI_3$ ($MAPbI_3$) perovskite. However, being a promising photovoltaic (PV) performance piloted by $MAPbI_3$, Pb-toxicity and poor stability obstructs the progress of PSCs in PV technology. In this regard, replacing Pb with some environmentally friendly, cheaper, and similar optoelectronic behaviour related alternative material or element is highly desirable. In this work, an attempt was made on copper as Cu (I) addition in the perovskite, $MAPbI_3$ through some exotic ways in an intention of Pb replacement, i.e., complete Pb replacement with Cu, which generates $MACu_xI_3$ ($1 \leq x \geq 2$); partial lead replacement, i.e., $MAPb_{1-x}Cu_xI_3$; and cocktail perovskite, i.e., both $MAPbI_3$ and $MACu_xI_3$ mixture, and finally they are employed for carbon-based perovskite solar cells. Remarkably, Cu incorporation facilitates the near-infrared (NIR) absorption, indicating a maximum solar spectrum absorbance. Integration of Cu as $MAPb_{1-x}Cu_xI_3$ resulting in the maximum PCE of ~12.85 %, whereas using 1:1 cocktail perovskite solution of $MAPbI_3$ and $MACu_xI_3$ exhibits an average PCE of ~12.43 %. On the other hand, during complete Pb substituted perovskites, $MACu_xI_3$, the device has only experienced an average PCE of ~4.0 %. However, $MACu_xI_3$-based PSCs lead to negligible PCE degradation as perceived up to 1000 hours, whereas Pb-based other devices are experienced rapid PCE depletion over the same period. Noticeably, Cu-incorporation facilitates a comparatively steeper and lesser PCE degradation rate than Pb-based PSCs. These results may help exploit unlimited possibilities of the potential application of Pb-free based highly stable solar cells and highlights the opportunities for broad solar absorption towards the NIR route and enhanced device stability. Besides, Cu employment has the advantages of environmentally benign impact, earth abundance, good thermal and aqueous stability.

Keywords: Perovskite Solar Cell; Lead-Free; Copper; NIR absorption; Photovoltaic; Stability

1. Introduction

The climate change caused by global warming can lead to significant concerns about human sustainability on earth; thus, it is essential to meet energy demands by reliable renewable energy sources rather than traditional fossil fuels to reduce global warming. Sunlight stands out as a viable alternative as a free energy treasure, eco-friendly, abundant in nature and economically cheap among all other renewable energy sources **[1,2]**. Perovskites as light-absorbing layers promise higher homogeneity and crystallization for better electrical performance to escalate the ultimate cell performance and reproducibility. Besides, third-generation solar cells are considered highly prospective for their contented, cost-effective and convenient fabrication approach for perovskite solar cells (PSCs) **[3**]. The dominant potential of PSC's is their easy solution processability than other silicon-based solar cells reported as highly stable, most efficient and standardize at the commercial level. Low-temperature processed can be helpful for energy payback time-moreover, the flexibility of design such as tandem solar cells manufacturing and fast processing. The most efficient PSCs are developed using $CH_3NH_3PbI_3$ ($MAPbI_3$) or analogous mixed cation lead-based hybrid halide perovskites. PSCs have already exhibited 25.2% of certified power conversion efficiency (PCE), which further elevated up to 29.5% in tandem devices with silicon **[4, 5]**.

Nevertheless, progress towards commercialization of the lead (Pb)-based perovskite photovoltaic (PV) technology retards due to poor thermal stability, rapid moisture ingression, and toxicity. Pb is carcinogenic and has no safe threshold limit of exposure, and it can cause severe toxicological implications on the environment with a dramatic impact on human health. Even the modification of the structure and further protection (encapsulation) of the perovskite absorber layer cannot prohibit the risk of Pb leakage into the environment **[6]**. Also, the isovalent substitution of Pb^{2+} position is a highly effective method for tuning perovskites' optical and electronic properties.

In this stage, searching for better non-toxic alternative candidates is highly demanding. The sought-after material is a good quality semiconductor with a suitable optical bandgap. The replacement of Pb by other divalent cations beyond group-IV elements turns out to provide a limited choice. Chemically speaking, one monovalent (M^+) and one trivalent (M^{3+}) ion are ideally suitable for two divalent Pb (II) ions replacement within the perovskite lattice. Elements like tin (Sn) or germanium (Ge) promises a better substitution, but the resulting compounds are found unstable and susceptible to oxidation **[7]**. Many attempts have been devoted to finding suitable substitution of Pb at $MAPbI_3$ structure to remove the toxicity. Nevertheless, that either resulted in a higher bandgap value (in the case of alkaline earth metals) which is unsuitable as an absorber material, or they turned out to be even more unstable **[8, 9]**.

Copper (Cu) addition can increase the light-harvesting efficiency of the light absorber by enhancing far-field scattering, increasing near-field local surface plasmons or as an agent to induce

charge separation. Consisting of high electronic conductivity and cheaper, Cu is a suitable element for Pb- substitution **[10, 11]**.

On the other hand, p-type materials as an alternate of lead as CuI in PV applications show promising results. Most of the same follow working mechanisms, including exciton generation. These excitons are relatively accessible, and intermolecular interactions can move between molecules freely until they are catch or decayed to the ground state. The charge separation procedure is initiated by exciting on separation [**12, 13**]. Introducing new light-harvesting materials, including Cu, that can utilize the near-infrared (NIR) spectrum signifies a considerable achievement. Broaden spectral absorption range of the materials leading to ample amount of coverage of solar spectrum resulting in higher photon harvesting develop the PV field to get exceptional PV results such as short circuit current and subsequent power conversion efficiency (PCE) of the devices [**14-16**].

The inherent advantages of NIR absorption of the active layer can consequently lead to higher PCE. In some cases, an inadequate photoelectric response at a longer wavelength and weak absorption at NIR wavelength is evident, possibly due to narrow bandgap material's carrier dynamics. The researchers have proposed numerous approaches to overcome these limitations to understand the procedure of exciton dissociation and incentive. However, materials with maximum absorption in a visible area, 50% of incident sunlight, lose thermalization and non-absorption photons. The improvement of the PV performance can be further developed by optimizing faster dye loading conditions and a tune to absorb NIR wavelength effectively **[17, 18]**.

CuI as p-type material has several distinctive properties to make its use favourable in PV applications to enhance the electrical and thermal performance of the systems. Cu-incorporation will also benefit PSC's stability resulting in 2% PCE loss after 170 h [**15**]. No diffusion of Cu into $CH_3NH_3PbI_3$ ($MAPbI_3$) has been observed after thermal annealing for over 100 hours at 80^{o}C, nor does it.

Cu generates charge trap states in direct contact with $MAPbI_3$ after long-term thermal annealing or illumination. Cu electrode retains 98% of the initial efficiency, which is > 20 % after 816 hours of storage in an ambient environment without encapsulation [**16**]. Cu is utilized with other materials such as CuI to be powerful candidates, such as implementing CuI as hole transport material [**17**]. The device's fill factor is also enhanced to 0.63 from 0.57 due to low series resistance, although the additional CuI layer in PSC [**18**]. Cu-doping leads to substantial changes to crystallinity enhancement, surface morphology improvement, energy level alignment optimization, trap densities reduction, and charge carrier recombination suppression in the perovskite films by incorporating the doping amount.

In this work, an attempt to reduce Pb toxicity with Cu addition has been executed in three possible ways such as i) complete Pb replacement, i.e., $MACu_xI_3$, ii) partial lead replacement, i.e., $MAPb_{1-x}Cu_xI_3$, and iii) cocktail perovskite, i.e., both $MAPbI_3$ and $MACu_xI_3$ mixture implementation for carbon-based perovskite solar cells. A preliminary electrical PV measurement has been performed for PSC employing the various Cu-associated perovskites at ambient. Results imply that the enhancement of electrical performance of device stability through Cu addition is more likely to arise

from electronic interactions mediated by charge transfer and inter-bandgap states increasing photoexcitation and extending surface-hole lifetimes along with the near infra-red broad absorption.

2. Experimental

2.1. Materials

The chemicals methylammonium iodide (CH_3NH_3I), copper iodide (CuI) and γ-butyrolactone were purchased from Merck Life Sciences, U.K. Octadecene (ODE, 90%), Oleic Acid (OA), and dimethylformamide (DMF) were purchased from Fisher Scientific, the U.K. All chemicals were used as received without further purification. Noticeably, during Cu incorporation into the lead (Pb^{2+}) replacement, CuI (Cu^{+}) is used because CuI_2 quickly decomposes to Cu (I) iodide with the release of I_2, as shown in Equation (1) and (2) **[19]**,

$$Cu^{2+} + 2I^{-} \rightarrow CuI_2 \quad (1)$$

$$2\ CuI_2 \rightarrow 2\ CuI + I_2 \quad (2)$$

2.2. Synthesis of $CH_3NH_3PbI_3$

The $CH_3NH_3PbI_3$ perovskite solution was prepared via an ion-exchange method. In short, 0.198 g CH_3NH_3I (Sigma-Aldrich) and 0.573 g PbI_2 (Sigma-Aldrich) were dissolved in 1 ml N-Methyl-2-Pyrrolidine (Sigma-Aldrich) and then stirred at 70 °C for 1 h before use.

2.3. Synthesis of $CH_3NH_3Cu_xI_3$

The oleate-chelation method achieved $CH_3NH_3Cu_xI_3$ through the colloidal synthesis approach (hot-injection method). This synthesis approach's advantage consists of (i) low-temperature reaction and (ii) oleate-chelation helps discrete nanocrystal formation **[20, 21]**. In this study, the $MAPb_{1-x}Cu_xI_3$ was synthesized by increasing Cu^{+} concentration (x) from 0.0 to 0.68 with a two-fold increment. Four (x = 0.02, 0.04, 0.08, 0.16. 0.32, 0.64) mixed halide hybrid perovskite ($MAPb_xCu_{1-x}I_3$) samples with different x values have been prepared. 0.556g of CH_3NH_3I in 2 ml OA and 25 ml ODE in a 100 ml three-necked flask with magnetic stirring and then heated to 120℃ for half an hour under an N_2 environment. Besides, 1.112g of CuI was dissolved in 5 ml of anhydrous γ-butyrolactone and then quickly injected into the three-necked flask and then heated to 135℃ to keep half an hour until the solution turned into dark brown. The obtained product was purified using 2ml of DMF to resolve the unreacted OA and ODE.

2.3. Preparation of cocktail perovskite

Synthesized $CH_3NH_3PbI_3$ and $CH_3NH_3Cu_xI_3$ have mixed in 1:1, 1:2, and 1:3 (v/v) using a magnetic stirrer in an intention to use more Cu-based perovskite and then stirred at 70 °C for 1 h before use.

2.4. Perovskite solar cell (PSC) fabrication

The carbon-based PSC devices are fabricated in an ambient environment with the mesoporous TiO_2 as the electron transporting layer and Al_2O_3 as the hole transporting layer. A preliminary attempt has been executed for carbon-based PSC employing all kinds of perovskite compositions at ambient conditions and understanding the possible influence of Cu incorporation on their electrical PV performance. As per our previous report, the PSC devices were fabricated, offering n-i-p configuration [**22, 23]**. In detail, TiO_2 compact layer was spin-coated on the etched clean fluorine-doped tin oxide (FTO) conductive glass by using 0.3 M titanium di-isopropoxide bis-(acetylacetonate) $Ti(acac)_2O^iPr_2$ (75 wt.% in isopropanol, Sigma-Aldrich) (99.9%, Sigma-Aldrich) solution in 2-propanol at 3000 rpm for 30 s, followed by drying at 115 °C for 5 min and cooled down to room temperature. This step was followed twice. The TiO_x coated samples were then placed on a hot plate and heated at 415 ± 10 °C for 30 minutes, then cooling to room temperature. The mesoporous TiO_2 layer was deposited by spin coating at 2000 rpm for 30 s using diluted TiO_2 paste (18NRT from Great cell Solar Company; w/w = 1:3.5 in ethanol) and heated at 500 °C for 60 min. After cooling down to room temperature, Al_2O_3 mesoporous layer was spin-coated with diluted Al_2O_3 paste (Sigma Aldrich; v/v = 1:2 in isopropanol) at 2000 rpm for the 30s and heated at 400 °C for 30 min. The mesoscopic carbon layer was finally screen-printed with the as-prepared carbon paste and sintered at 450 °C for 30 min. Carbon paste preparation details can be found in our previous report **[22]**. All the following processes were executed at ambient and without employing a glove box. The humidity during the fabrication of the PSC device was ~50–60%.

Finally, the prepared perovskite precursor solution (20 µl) as mentioned above was infiltrated by drop-casting via the top of the carbon counter electrode and further spin-coating at a speed of 1000 rpm for kept at 50°C for 1 h and finally used for electrical measurements. The overall experimental process has been schematically described in **Fig. 1**.

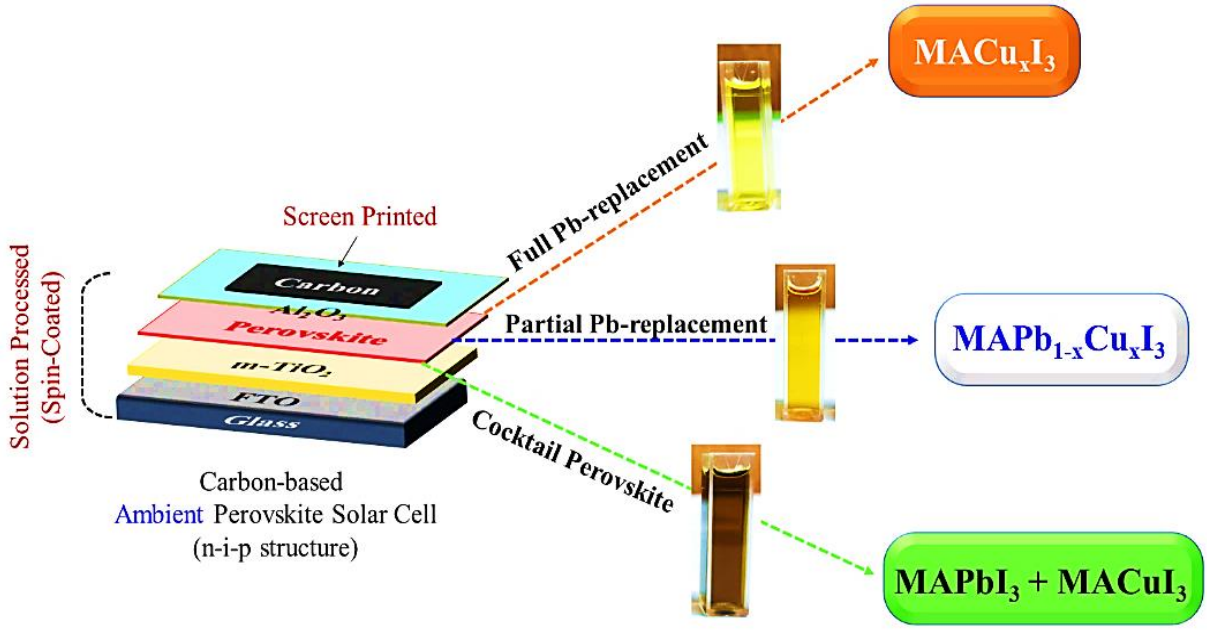

Fig. 1. Schematic diagram of possible Cu-incorporation in $MAPbI_3$-based ambient perovskite solar cells.

3. Material characterizations

The structural properties of the prepared perovskite thin films were characterized by using a Bruker D8 Advance X-ray diffractometer (Billerica, MA, USA). A PerkinElmer Lambda 1050 UV/vis/NIR spectrophotometer was used to measure the absorbance for the spin-coated perovskite's thin-film samples. The microstructure of the synthesized perovskite thin-films was characterized using a scanning electron microscope TESCAN VEGA3 SEM coupled with energy-dispersive spectroscopy (EDS) from Oxford instrument elemental analysis. The PV measurements of the fabricated devices were executed under 1000 $W.m^{-2}$ light from a Wacom AAA continuous solar simulator (WXS-210S-20, AM1.5G) **[22, 23]**. The photocurrent density-voltage (J-V) characteristics of the devices were recorded using an EKO MP-160i *I-V* Tracer. PV measurements were carried out for ten PSC devices consisting of an active area of 0.16 cm^2. Electrochemical impedance spectroscopy (EIS) measurements were carried out under the solar simulator condition with the frequency range from 0.1 Hz to 100 kHz with an AUTO LAB PGSTAT 10. Besides, the same devices were tested for the incident photon to current efficiency (IPCE) using the BENTHAM PVE300 Photovoltaic EQE (IPCE) and IQE solution under 300-1100 nm wavelength.

4. Results and discussion

4.1. X-ray diffraction analysis of the synthesized perovskite thin-films

XRD characterization has been performed to identify the phases present in all the prepared perovskite samples. The XRD patterns of the $MAPbI_3$ sample shown in **Fig. 2** indicate the existence of all the expected compounds. The calculated lattice parameter with a = 8.789 Å and c = 12.567 Å, along with all the obtained diffraction peaks, were well-agreed with the tetragonal crystallographic structure at room temperature **[24]**. The most intense peak of (110) of the tetragonal perovskite lattice further deciphered that the (110) crystallographic domains act as pillars and are strongly supported for building/ crystallites tetragonal crystal structure. The XRD results in the preliminary $MACu_xI_3$ ($1 \leq x \geq 2$) phase have been compared with the MAI and CuI. Thus, they ruled out any of its precursory phases and possibly generated the desired perovskite phase. We found experimentally there is no report yet to confirm $MACu_xI_3$ structure; this is probably due to unavailability of Cu(II) iodide or forming Cu_xI_x complex instead of desired perovskite phase and thus unable to decide the actual crystalline planes originated for this sample **[25]**. As a result, we proposed the Cu(I) replacement to $MAPbI_3$ structure could generate the $MACu_xI_3$ ($1 \leq x \geq 2$) phase. While, $MACu_xI_3$ is expected to form highly stable and perfect cubic structure perovskites since its tolerance factor is ~0.972, within the range of 0.89-1.0 **[26]**. At the same time, the results of theoretical calculations show that Cu can form stable perovskite structures **[27, 28]**. However, the observed peaks of the $MACu_xI_3$ could be due to more counts accumulated in this orientation, leading to dominancy in the polycrystalline material with a tetragonal system. Instead of Cu^{2+} ion, Cu^{+} ion is replacing the Pb^{2+} ion in the perovskite crystal, and therefore it is anticipated that either Cu deficient phases can be evolved when the reaction is executed for $MAPb_{1-x}Cu_xI_3$ **[29]**. The strong characteristic diffraction peaks located at 12.8°, 13.6°, and 25-30° zone in the XRD pattern of $MAPb_{1-x}Cu_xI_3$ corresponds to the (110), (220) and (310) crystal planes of the tetragonal perovskite structure, respectively, and the (110) plane is preferentially oriented, which is consistent with previous work **[30, 31]**. This is probably due to the ionic radii of Cu(I) (74 pm) is much lower than ionic radii of Pb^{2+} (120 pm) and I^{-} (216 pm), and thus cause the diffraction peak of $MAPbI_3$ move to a lower angle. While in the case of the $MAPb_{1-x}Cu_xI_3$ sample, some additional peaks of CH_3NH_3I and CuI are also detected due to the preferential exposure of crystalline impurity **[32]**. The intensity of the $MAPbI_3$ characteristic peaks gradually decreased with increasing full width at half maximum when Cu was introduced in the $MAPb_{1-x}Cu_xI_3$ sample.

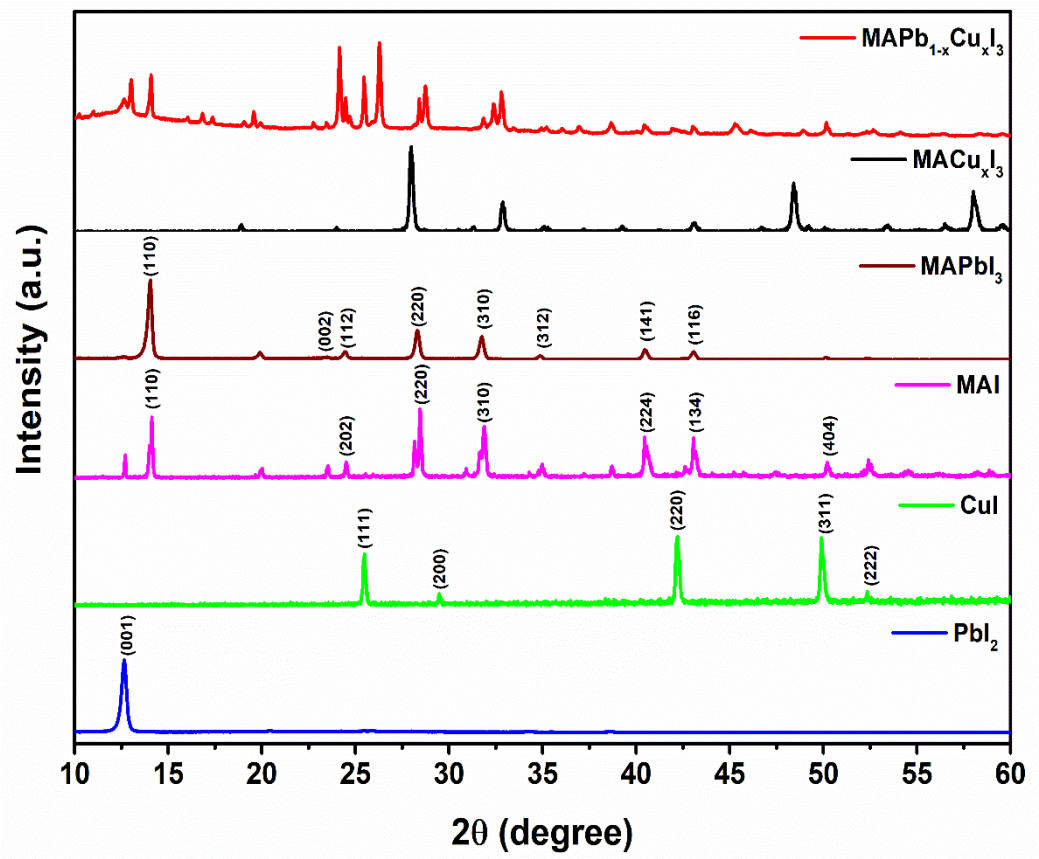

Fig. 2. XRD pattern of the prepared perovskite samples.

4.2. Optical absorption spectra analysis of the synthesized perovskite thin-films

The absorbance spectral is shown to 1200 nm, shown in **Fig. 3a and Fig. 3b.** It can be seen from the higher absorbance spectrum at a shorter wavelength followed by a reduction in absorbance with a broad localized surface plasmon resonance in the NIR region for synthesized $MACu_xI_3$ sample, as shown in **Fig. 3a**. Interestingly, $MACu_xI_3$ showed absorption in the NIR region raging 780-1200 nm, which generated a strong tendency that ultimately benefitted for device's PV properties due to the maximum solar spectrum coverage **[33]**. A sharp absorption edge at ~480 nm along with a new tail absorption edge at ~1150 nm (NIR range) is observed. The optical bandgap energy of the perovskite was determined by extrapolating the linear regions of the plots of $(\alpha h\nu)^2$ versus photon energy ($h\nu$), i.e., Tauc Plot. Cu^{2+} incorporation resulted in bandgap tuning from 1.22 to 2.99 eV. These values fall in the range of optimum band gaps for the light absorbers in thin-film solar cells.

Besides, the $MAPb_{1-x}Cu_xI_3$ composite perovskite exhibits a broad absorption spectrum starting from ~600 nm and extended up to ~1100 nm, showing a maximum absorption peak at ~682 nm and a new tail absorption edge ~1050 nm, as shown in **Fig. 3b**. Due to the consistent $3d_{10}$ electronic configuration, Cu(I) cannot exhibit the widespread Jahn-Teller distortion, which is very common for Cu (II) ions. However, the large polarisability of the I^- ion and $MACu_x$ complex could propagate the room-temperature absorption spectra of $MACu_xI_3$ towards low-energy-lying metal charge transfer (MLCT)

bands distortion of the CuI_6 octahedra **[32]**. Cu^I center also transfers the photons to the MA's low-lying π* orbitals **[35]**. Besides, I- could influence the free electrons in the conduction band of $MACu_xI_3$, which contributes to intense surface plasmon absorption in the NIR region, followed by the Burstein-Moss effect. All these phenomena lead to extend the absorption towards the NIR **[36]**.

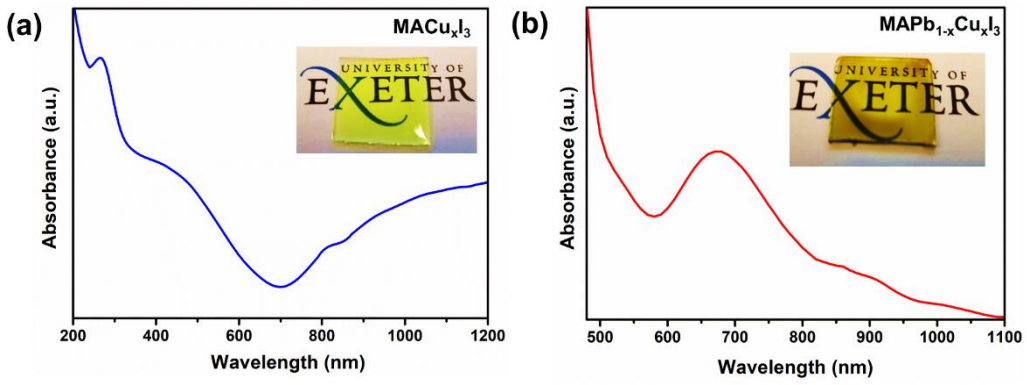

Fig. 3. The absorption spectrum of (a) $MACu_xI_3$ and (b) $MAPb_{1-x}Cu_xI_3$ samples, respectively. (Inset: photographs of corresponding thin films).

4.3. Scanning electron microscope evaluated microstructures and corresponding elemental mapping analysis of the synthesized perovskite thin-films

Fig. 4a-c exhibits SEM images of the $MACu_xI_3$ perovskite films at different magnifications in the form of one-dimensional (1D) rod-spindle kind morphology. The SEM images of perovskite material exhibited densely packed elongated rod type morphology with a length of 200 nm to 1 µm and an average width of 15 ± 2 nm, as shown in **Fig. 4(c)**. A spindle-like structure with irregular distribution was formed with the preformed bunch of rods elongated from the centre outwards. Similarly, SEM microstructure analysis for $MAPb_{1-x}Cu_xI_3$ sample was also performed at different magnifications, as shown in **Fig. 4d-f**. In this case, the SEM microstructure analysis reveals wafter kind morphology consisting of fibre networking patterns. The structure is consisting a length of 500 nm to 2 µm and an average width of 25 ± 2 nm, as shown in **Fig. 4(f)**. No other surfactant or stabilizer was used in the synthesis procedure except the precursor solution to grow this kind of 1D nanostructures. Low magnification SEM images signify that the thicker bundles get dispersed and separated. A much closer examination of individual 1D nanostructures could be observed where the perforated surface of the rods is evident. The tips of the rods are tapered, while the rest of the constitution is quite similar to a flattened strip.

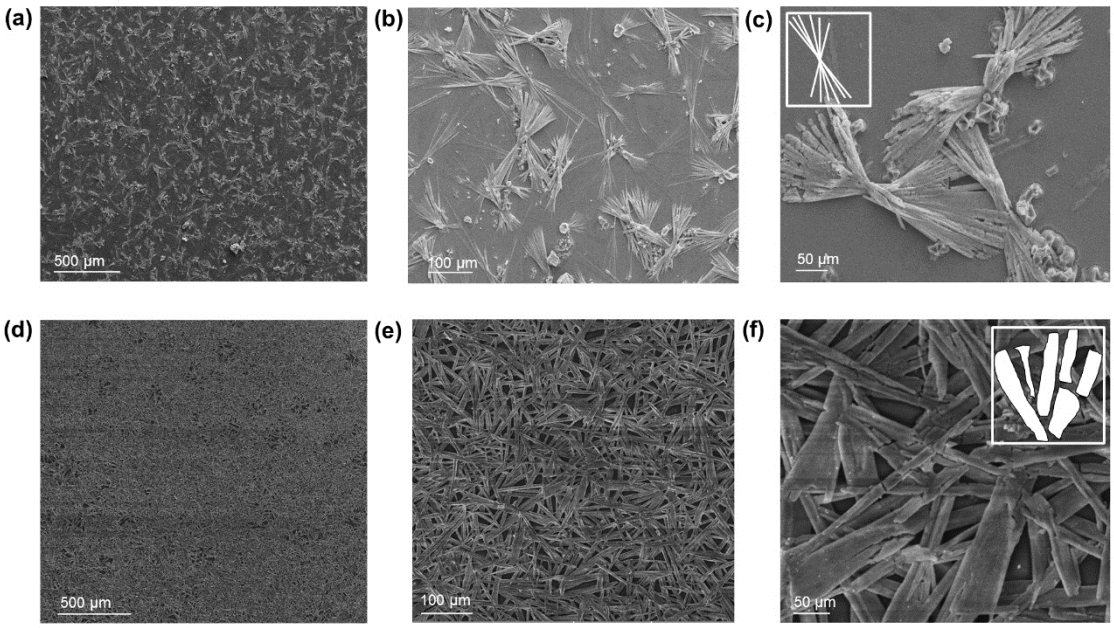

Fig. 4. SEM microstructural images of (a)-(c) MACuxI3 and (d)-(f) $MAPb_{1-x}Cu_xI_3$ perovskites at different magnifications, respectively. Inset pictures portrait the type of corresponding nanostructured formation.

The EDS colour mapping elemental analysis from SEM was executed with the synthesized perovskite of the $MACu_xI_3$, and $MAPb_{1-x}Cu_xI_3$, as shown in **Fig. 5a** and **Fig. 5b**, respectively. The results indicate the elemental distribution showing the homogeneous distribution with distinct color contrast of all the compositional elements for $MACu_xI_3$ and $MAPb_{1-x}Cu_xI_3$ shown in **Fig. 5a**. Besides, **in Fig. 5b,** the Cu existence in the core region of $MAPb_{1-x}Cu_xI_3$ in the structure has been well spotted.

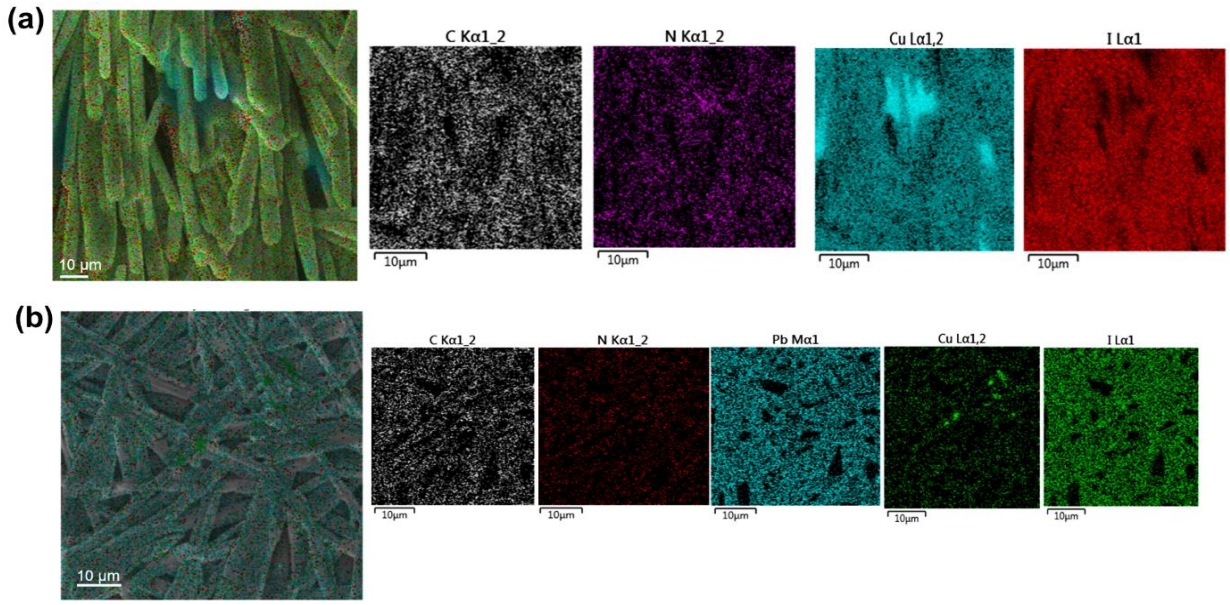

Fig. 5. EDS elemental mapping images of (a) $MACu_xI_3$ and (b) $MAPb_{1-x}Cu_xI_3$ perovskite samples, respectively.

4.4. Study on the absorbance behaviour for Cu-doping $MAPb_{1-x}Cu_xI_3$ *and cocktail perovskite samples*

Fig. 6a represents the absorption spectra of the $MAPb_{1-x}Cu_xI_3$ samples, where the Cu concentration (x) varies from 0 to 0.68. While increasing the Cu concentration, the intensity of absorption spectra for the $MAPb_{1-x}Cu_xI_3$ sample is significantly improved, and it is almost saturated for the $MAPb_{1-x}Cu_xI_3$ sample when the x reaches 0.68. Interestingly, all the spectra comprise a broad absorption range of 500 nm to 1100 nm and exhibit a maximum absorption at ~670 nm. The comprehensive nature and high intense absorption characteristics of $MAPb_{1-x}Cu_xI_3$ samples further allow them as a superior light-absorbing material for PSC. However, in the case of cocktail perovskite, where $MAPbI_3$ and $MACu_xI_3$ have been mixed in various (v/v) ratios resulted in an extensive absorption towards the NIR zone, as shown in **Fig. 6b**. $MACu_xI_3$ contains both visible and NIR absorption while adding $MAPbI_3$ into it, leading to a bathochromic shift of the visible band followed by a reduction in the NIR absorbance that originated for $MACu_xI_3$. While increasing the amount of $MACu_xI_3$ to $MAPbI_3$ does not lead to further absorbance enhancement, the absorption significantly subsided to 10%. In this respect, it is expected that 1:1 mixing of $MACu_xI_3$ to $MAPbI_3$ cocktail perovskite would perform superior for PSC application compares to its other counterparts. **Fig. 6c** represents the maximum light absorption variation recorded at 670 nm regarding different Cu concentrations for the $MAPb_{1-x}Cu_xI_3$ sample. Once the Cu concentration reaches 0.3, the light absorption of the $MAPb_{1-x}Cu_xI_3$ solution gets saturated. This indicates, increases the amount of Cu does not guarantee more light absorption, and thus an optimum concentration is required that condemn better PV performance. It is anticipated that the expeditious absorbance decay processes are leaded by nonradiative recombination of electrons and holes through defects or trap states in the cocktail perovskite, which is similar to obtained in Sn/Pb

cocktail perovskite **[37-39]**. **Fig. 6d** displays the photograph of visual colour change concerning an increase of Cu doping concentration. A distinct colour change is visible when the Cu concentration increases from 0.32 to 0.64. A high concentration of Cu inclusion also lowers the transparency, which can restrict electron excitation.

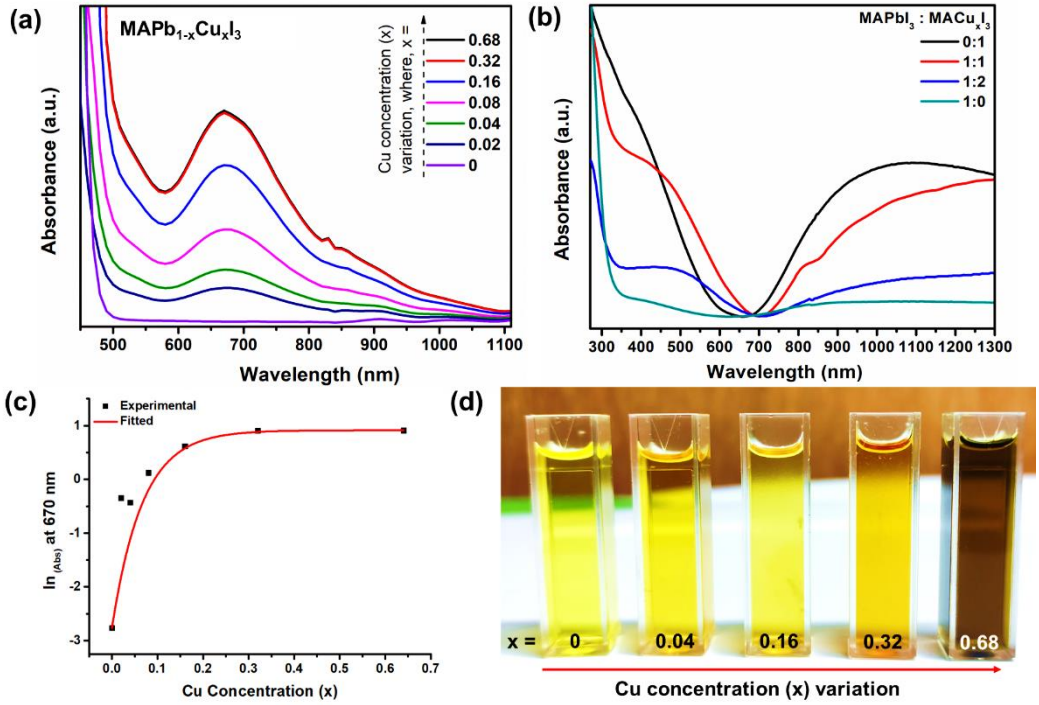

Fig. 6. Absorption spectra of (a) $MAPb_{1-x}Cu_xI_3$ where x represents Cu concentration which is varied from 0 to 0.68, and (b) cocktail perovskite prepared with mixing of $MAPbI_3$ and $MACu_xI_3$ perovskite solution in different (v/v) ratio, respectively, (c) a logarimetric plot of $MAPb_{1-x}Cu_xI_3$ samples with respect of their different Cu concentration, and (d) corresponding photograph image.

4.5. Photovoltaic performance and device stability study

The results obtained from Cu-based perovskite confirm the promising ability of light-absorbing material characteristic for PSC application. Therefore, the photovoltaic performance of three different perovskite employed devices are finally investigated in an ambient environment. The photocurrent-voltage (J-V) features of all three devices are illustrated in **Fig. 7a**. As shown in **Fig. 7a**, the J-V features of the $MAPb_{1-x}Cu_xI_3$-based PSC exhibit a short circuit current density (J_{SC}) of ~20 $mA.cm^{-2}$ and with an open-circuit voltage (V_{OC}) of ~900 mV, resulted in the highest PCE of ~11.0 %. The J_{SC} dropped to 16.83 $mA.cm^{-2}$ of J_{SC}, keeping the V_{OC} almost similar to $MAPbI_3$-based PSC showing the highest PCE of ~8.75%. At the same time, $MACu_xI_3$-based PSC exhibits comparatively lesser J_{SC} (7.32 $mA.cm^{-2}$) than the other counter PSCs resulting in the highest PCE of ~4.0%. However, noticeably the V_{OC} remains almost fixed all the devices while the J_{SC} rapidly varies. The devices' V_{OC}, J_{SC}, and PCE are observed from the J-V characteristic curve and PCE comparative plot. The fill factor (FF) of the devices is also measured, which is an excellent way to quantify the electrical output of the PV devices. All the PV

parameters are tabulated in **Table 1**. **Fig. 7b** illustrates the PCE trend of a similar set of devices, which do not result in >2% error during the measurement.

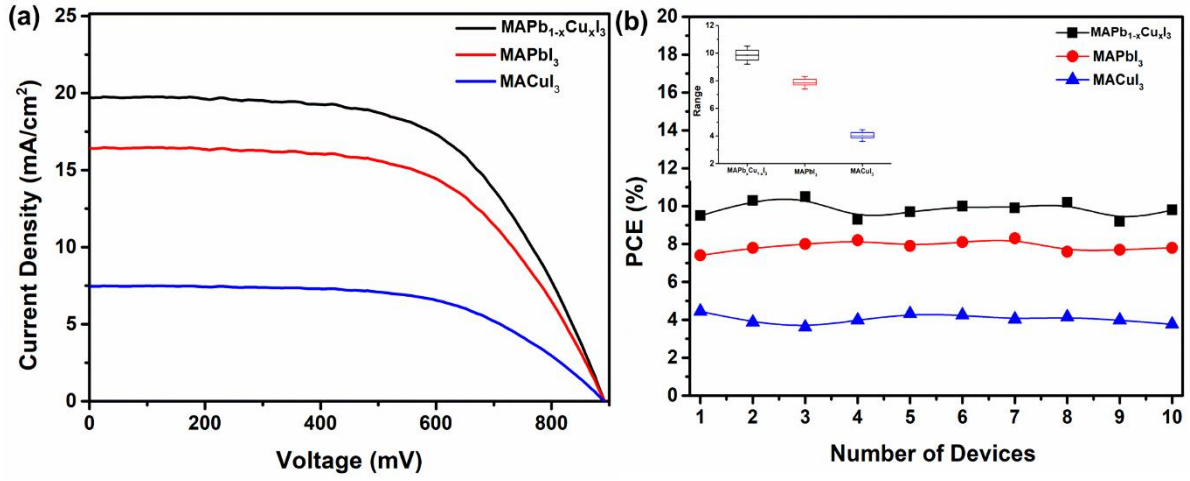

Fig. 7. (a) current density vs voltage plot for the various perovskites employed PV devices, (b) plot of average PCE determination using a similar set of PSCs. (Inset: corresponding error bar plot).

Table 1. Photovoltaic parameters of different perovskite-based PV devices

Perovskite	**J_{SC} (mA. cm^{-2}) ± 1.5**	**V_{OC}(mV)**	**FF**	**Average PCE$^{\#}$ (%)**
$MAPbI_3$	16.48	901	0.59	8.75
$MACuI_3$	7.32	900	0.60	4.01
$MAPb_xCu_{1-x}I_3$ (x = 0.68)	19.83	900	0.61	11.05

The J-V characteristic of the device following configuring of $MAPb_{1-x}Cu_xI_3$-based PSC with varying amounts of Pb and Cu in the light-absorbing layer is measured as shown in **Fig. 8a**. The maximum amount of Cu having 0.32 content showed a maximum of ~24 mA.cm^{-2} of J_{SC}. While, for the amount of Cu (x)= 0.68, 0.84, 0.92, 0.96, J_{SC} observed to be 22.64 mA.cm^{-2}, 19.68 mA.cm^{-2}, 17.79 mA.cm^{-2} and 16.47 mA.cm^{-2} respectively with almost fixed amount of V_{OC} of ~900 mV. The highest efficiency resulting from the $MAPb_{1-x}Cu_xI_3$-based PSC device is 12.85 %, with the Cu concentration 0.68. The photovoltaic performance $MAPb_{1-x}Cu_xI_3$-based PSC exhibits significant enhancement of J_{SC} with the increasing amount of Cu-concentration, while the V_{OC} experiences an insignificant change.

In the case of cocktail perovskite-based devices, the PV characteristics significantly change once the $MACuI_3$ addition to the $MAPbI_3$. In **Fig. 8b**, it has been observed that the enhancement ratio of $MACu_xI_3$ to the $MAPbI_3$ is noticeably reduced in both the J_{SC} and V_{OC} of the devices, while FF remains almost unchanged. The highest efficiency was achieved for 1:1 $MACu_xI_3$ to the $MAPbI_3$ cocktail perovskite leading to the PCE of ~12.43 %. Corresponding PV parameters are summarized in **Table 2**.

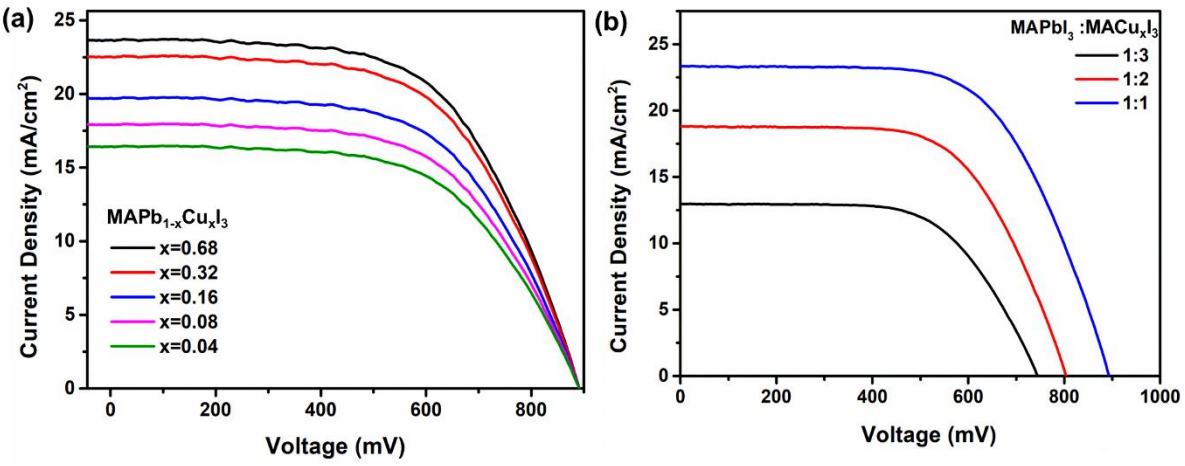

Fig. 8. Current density vs voltage plot for the (a) $MAPb_{1-x}Cu_xI_3$, (b) cocktail perovskite ($MAPbI_3$: $MACu_xI_3$)-based PV devices, respectively.

Table 2. Photovoltaic performance of $MAPb_xCl_{1-x}I_3$ and cocktail perovskite-based devices, respectively.

$MAPb_xCu_{1-x}I_3$-based devices				
$MAPb_xCu_{1-x}I_3$ (x=)	**J_{SC} (mA. cm^{-2}) ± 0.5**	**V_{OC}(mV)**	**FF**	**Average PCE[#] (%)**
0.04	16.47	895	0.61	8.92
0.08	17.79	892	0.60	9.36
0.16	19.68	894	0.60	10.35
0.32	22.64	892	0.61	11.91
0.64	23.72	893	0.60	12.85
Cocktail perovskite-based devices				
$MAPbI_3$: $MACuI_3$	**J_{SC} (mA. cm^{-2}) ± 0.8**	**V_{OC}(mV)**	**FF**	**Average PCE[#] (%)**
0:1	7.32	900	0.60	4.01
1:1	23.51	901	0.61	12.43
1:2	18.83	803	0.61	8.92
1:3	12.98	7.44	0.59	5.70
1:0	16.48	901	0.59	8.75

So, based on the preliminary PV performances of different Cu-based perovskites devices, accelerated a significant change in the photocurrent density for all the cases. Besides, there is a V_{OC} dropping during Cu concentration enhancement for cocktail perovskites. The trade-off between J_{SC} and V_{OC} is replicate in terms of different Cu incorporation amounts in **Fig. 9a**. The average PCE of all four devices with varying periods is estimated, as shown in **Fig. 9b**. The device with mixed content of Pb and Cu signified a maximum of 12.85 % of PCE attributed to higher trap density which fell to ~1% after 1000h after exposure. The device with varying amounts of Pb and Cu indicated ~11 % of PCE with a decline of ~3% after 1000h of exposure. In contrast, the device with a partial Pb exhibited PCE of ~8%, which diminished to ~2% after the same period. However, the $MACu_xI_3$ (Pb free) device does not show any

degradation and remains stable at ~4%, indicating a promising route for stability without any degradation.

A small effect of hysteresis is perceived for all the Pb devices except Cu incorporation within PSC devices. However, efficiency with a more negligible hysteresis effect was observed for the under-investigated copper-based PSC device due to the material's transition nature and recombination phenomena within cells. It is worth noting; all the devices are tested in the ambient environment in the presence of air without any further encapsulation. For the PSC devices operated in such an environment, a little bit of degradation is evident. Moreover, the structure of the devices also plays a vital role in estimating the obtained efficiency. $MACu_xI_3$ enhances its stability against oxidation and the use of a dedicated device stack that minimizes interfacial recombination. However, the organic counterpart (MA) is quite unstable due to the irreversible degradation of volatile MA cation being a promising opto-electrical candidate [**40**]. Thus, perovskite without volatile components became a necessary route, which opened many possibilities for futuristic research.

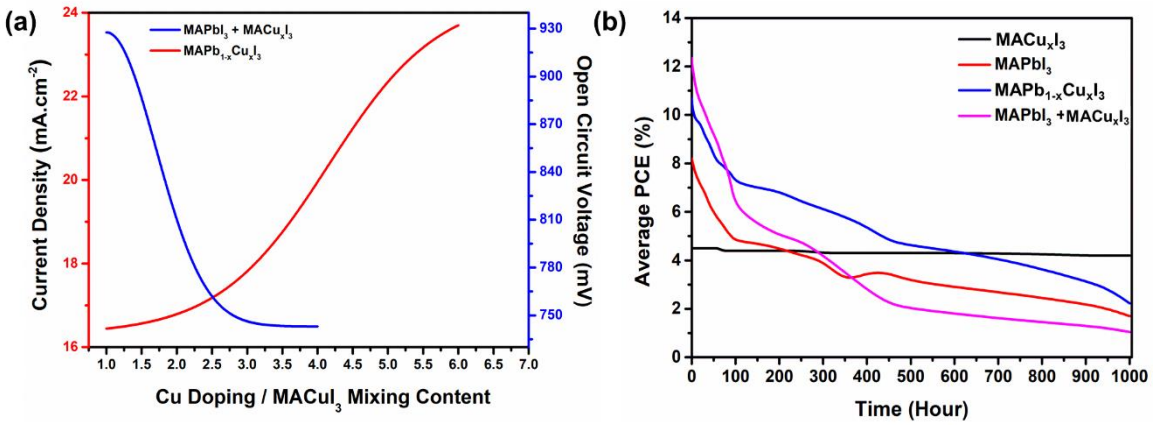

Fig. 9. (a) Plot of Current density and voltage observed during the PV measurement for different Cu-concentration or mixing contact varied PSCs, (b) stability plot recorded up to 1000 hours for different perovskite employed PSC devices.

4.6. Electrochemical impedance and incident photon to current conversion efficiency spectra analyses

The Electrochemical impedance spectroscopy (EIS) measurements were conducted with the PSC devices to understand the transport properties of Cu addition at different interfaces. The EIS recorded Nyquist plots in **Fig. 10a** indicates the shortest series resistance (R_S) of 26.33 $\Omega.cm^{-2}$ and electrochemical charge transfer resistance (R_{CT}) of 686.51 $\Omega.cm^{-2}$ for $MAPb_xCu_{1-x}I_3$-based PSCs compared to the other perovskite devices. The $MACu_xI_3$-based PSC shows the highest R_S and R_{CT} values, 89.65 and 1206.24 $\Omega.cm^{-2}$, respectively. The partial replacement of Pb with Cu gives the smallest R_S and RCT value, which reflects a good bonding strength

between TiO_2/perovskite/Al_2O_3 interface. Further, it promotes more electrons from the external circuit, thus leading to the highest PCE.

Besides, the IPCE measurements were also performed within the wavelength of 300 - 1100 nm for the same devices, and their corresponding plot is shown in **Fig. 10b**. The IPCE curve for $MAPb_xCu_{1-x}I_3$-based PSC exhibits the highest IPCE value of ~80%, which is ~8% enhancement of $MAPbI_3$-based PSC. Interestingly, the $MACu_xI_3$-based PSC shows a broad IPCE curve extended to 1100 nm with a comparatively lower IPCE value of ~40%. However, the IPCE curve pattern of the $MACu_xI_3$-based PSC was observed as unique, and at the same time, with an extension to the NIR wavelength, corroborates with its absorption results. In contrast, due to the lesser IPCE value, the PCE resulting from the $MACu_xI_3$-based PSCs are pretty low compared to the lead-based devices. This indicates complete removal of Pb with Cu reduces the current, even the absorption range extended to NIR wavelength, generating more trap states of electron recombination **[41]**.

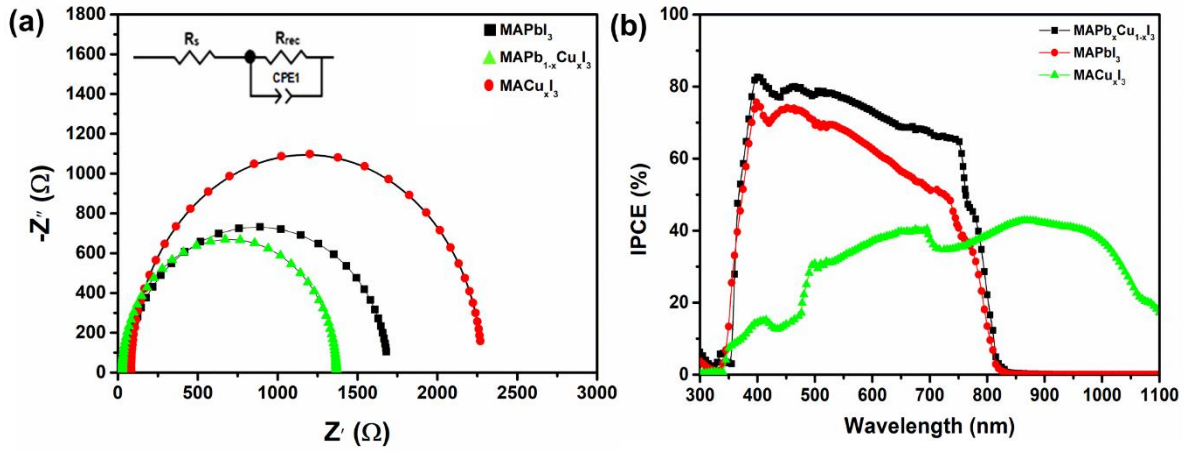

Fig. 10. (a) Nyquist plot (inset: corresponding equivalent circuit of the all the fitted devices) and (b) IPCE curve for the $MAPb_xCu_{1-x}I_3$ and $MACu_xI_3$-based PSCs compared with $MAPbI_3$-based PSC.

4.7. Band alignment and relative discussion regarding Cu-incorporated perovskite solar cells

Fig. 11a represents the bandgap positions of each layer of the PSC device. In this work, Cu has been incorporated in many ways, so it is believed that the insertion of the Cu similar to the CuI buffer layer is supposed to effectively reduce the energy level mismatching between the transport layer and absorption layer **[42]**. Utilizing this advantage of Cu-doping, the device may reduce the loss of voltage and photocurrent. Besides, Cu-incorporation sometimes provides a surface modification of TiO_2-layers where it could drag out the electrons toward the perovskite/TiO_2 interface, resulting in a shift of the energy levels and superior electron

extraction with a low trap density **[43]**. However, overusing Cu blocked the electron conduction pathway, and as a result, the PCE becomes either saturated or decreased (**Fig. 11b**).

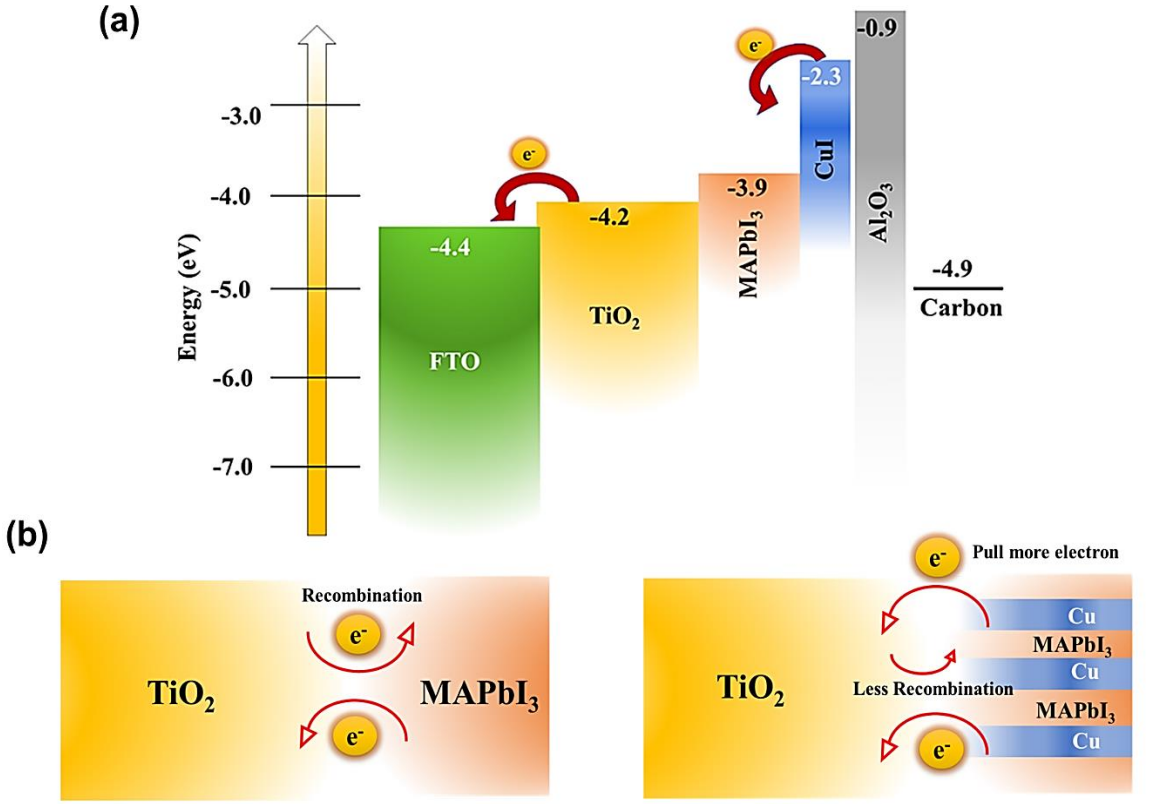

Fig. 11. Schematic representation of (a) band alignment position for the carbon-based perovskite cell, (b) Cu addition impact on electron-hole recombination occurring at perovskite/TiO_2 interface.

It is anticipated that forming a relatively better charge transport channel across the Cu-I network for Cu- added perovskites enhances the electron mobility rate resulting in photocurrent enhancement. This is probably due to the lower electronegativity difference fitted with Goldschmidt's tolerance rule along the Cu-I bond can also lead to a lower bandgap desired for visible and NIR range optoelectronics. Increased covalency of the Cu-I bond compared to the Pb-I bond is consistent with Cu's lower electronegativity than Pb, which signifies the feasibility of this type of perovskite formation, which is exactly predicted for chalcogenide-based perovskites as well **[44, 45]**. Also, preliminary experiments already demonstrated superior long-term stability when incorporating CuI as a hole transport layer for PSCs **[46]**. However, Cu-concentration on the perovskite structure formation is crucial. The improvement of photovoltaic properties was attributed to the partial substitution of Cu at the Pb sites, as seen from the previous reports. For example, Ahmed et al. (2020) recently reported Cu(II)-based perovskites

for $C_6H_4NH_2CuBr_2I$ and $C_6H_4NH_2CuCl_2I$ as light absorbers for the development of Pb-free PSCs. However, the PCE obtained using these perovskites are very low (<1%) **[47]**. Cu(II) based perovskites exhibit lower efficiency due to lesser carrier transport and higher electron recombination rate. However, they showed better stability and enhance photocurrent density. This is similar to observed for $MASnI_3$, where Sn^{2+} replaced Pb^{2+}. A maximum PCE of 6.79% was achieved in using $MAPbCu_xI_{1-x}$, where = 0.17 -based perovskite by Shirahata et al. (2017) **[29]**. In addition, Cu doping up to 20% would increase the density of defects and hole traps in the NiOx, leading to massive enhancement of the device performance, particularly for the Voc, FF, and hole mobility **[48]**. Besides, $(MA)_2CuCl_4$ yielded a PCE (η) of 2.41%, whereas they were 1.75% and 0.99% for $(MA)_2CuCl_2I_2$ and $(MA)_2CuCl_2Br_2$, respectively.

Cu^{2+} reduction caused by the higher trap density can explain the lower performance of $(MA)_2CuCl_2Br_2$ **[25]**. The low efficiency achieved for copper-based PSCs may come from forming Cu^+ trap states during the film formation. Still, the good thing behind using copper-based lead-free perovskite devices is the efficient luminescence coming from in situ formed Cu(I) ions. The origin of the $MACu_xI_3$ or $MAPb_{1-x}Cu_xI_3$ formation is still unclear. At the same time, the preliminary photovoltaic results signify that complete removal of Pb is responsible for significant PCE loss that can be observed from $MACuI_3$-based PSCs. In Cu doping or cocktail perovskite, the initial PCE is almost triple that of the $MACu_xI_3$-based PSCs. Of course, Pb will always remain a toxic element; however, innovative chemistry approaches through a cheaper and efficient way like Cu-addition can suppress the chances of lead toxicity and retain the excellent performance of PSCs **[49]**.

However, so far, no reports exist on the successful synthesis of CuI-based perovskites. Therefore, it is challenging to declare the coordination state of Cu^+ for insane. The smaller ionic radii of Cu+ are unable to form $CuBr_6$ and CuI_6 octahedra. Besides, Cu $3d^{10}$ electrons are underlying in high energy levels and quite unstable. As a result, a strong hybridization is thermodynamically favourable between Cu 4s and 4p to lower the energy. A lower coordination number leads to a more significant distortion on the d^{10} orbitals and, therefore, more robust d-s and d-p hybridization **[50]**. As a result, many studies reveal a high tendency of two or three-dimensional layered perovskite formation while using the Cu^+ incorporation. Xiao et al. (2017) proved using both the experimental and theoretical consideration of Cu^+ halide double perovskite's synthesis under thermal equilibrium conditions, leading to products with 4-fold coordinated Cu atoms **[50]**.

On the other hand, alloying of Cu^+-In^{3+} coordination spheres can pack most favourably into a two-dimensional footprint of the inorganic sheets leading to mixed-valence layered halide stable perovskite structure **[51]**. The specific semiconducting properties of Cu^+-In^{3+} was also

revealed by Bi et al. (2020) **[52]**. All these studies signify that incorporating Cu(I) can stabilise the Pb^{2+} perovskite structure while alloying with other metal ions. Therefore, to understand the structural information of Cu(I)-based perovskite for this work, the computational and experimental material design challenges need to be addressed.

Still, they appear to be due to defect states and improper nucleation, perhaps due to local differences in surface charge or impure phases or with stress induce delamination. However, the Cu-based perovskites open a new side of research to this file. Still, most of the studies in the literature are restricted to theoretical work or generate less efficiency. However, the excellent agreement with various theoretical studies of lead-free perovskite compounds lends credibility to the approach. High PCE keeping the lead-free perovskite utilization will be achieved by mastering multiple manufacturing challenges, such as developing planar n-i-p, p-i-n, inverted, mesoporous architectures. We believe computational and experimental material design challenges need to be addressed for this type of perovskites **[53]**.

5. Conclusions

In this work, Cu is added in the popular perovskites, $CH_3NH_3PbI_3$, in an intention of Pb-replacement, which does not contain the environmentally benign impact, and has good thermal and aqueous stability. In order to replace Pb, we have added Cu(I) ion in their different possible ways, such as complete replacement of Pb, which turned into $MACu_xI_3$, partial replacement of Pb resulting in $MAPb_xCu_{1-x}I_3$ perovskite, and a cocktail perovskite combination of $MAPbI_3$ and $MACu_xI_3$ perovskites as light harvesters for perovskite solar cell application. During the X-ray diffraction analysis, we are not confident about the same phase formation of $MACu_xI_3$, i.e., complete replacement of Pb. This is because CuI_2 is unstable and rapidly reduced to CuI. However, we find the observed X-ray diffractions pattern contains none of their precursor peaks and therefore indicate a strong possibility of some complex formation when CH_3NH_3I and CuI are reacted. However, Cu incorporation enhances the absorption towards the NIR region. Thus, the bandgap engineering of Cu added perovskite was reported covering much of the visible spectrum and NIR. The morphology of the Cu added perovskites are also quite interesting, forming rod and stripes type 1D structures within a diameter of 20-30 nm. After synthesizing the perovskite sets, we have applied them to the perovskite solar cell application to evaluate their PV performance. The highest efficiency achieved by the PSC devices with $MAPb_xCu_{1-x}I_3$ perovskite was ~12.85 %, while $MACu_xI_3$-based PSCs exhibited the highest efficiency of ~4.0%. Interestingly, Cu addition significantly increases the photocurrent density while V_{OC} remains almost identical for $MAPb_xCu_{1-x}I_3$ -based PSCs. Whereas, in the case of cocktail perovskites, adding more Cu to Pb perovskites resulting a reduction of both photocurrent density and voltage. Also, we observed all the PSCs stability up to 1000 hours of ambient exposure, and

remarkably $MACu_xI_3$-based PSC retained its initial efficiency with a minor degradation. In contrast, Pb-Cu both included perovskites relatively degraded fast and lost their initial efficiency > 90% during the exposure.

However, we observed complete replacement of Pb with Cu unable to show the similar efficiency like Pb-based devices. In contrast, partial replacement of Pb with Cu either through doping or utilizing cocktail perovskite elevated to the PCE compare to the $MAPbI_3$-based device. We believe possible Cu addition to $MAPbI_3$ perovskite and their preliminary PV performances reported a critical step toward realizing cost-effective, highly efficient, environmentally friendly solar cells. Pb-free perovskites and their relative derivatives exhibit various imperative properties that make them appealing in photovoltaics and a broad scope of various optoelectronic and photonic applications. Some initial studies found promising, but more attention is needed to achieve inventive progressions in the photovoltaics area. A correlation of theoretical simulations and experimental discoveries for lead-free new perovskite material's research paves the way for the high-efficiency Pb-free PSCs.

CRediT authorship contribution statement

Maria Khalid: Formal analysis, Investigation, Writing-original draft, **Anurag Roy:** Conceptualization, Methodology, Investigation, Writing-review & editing, validation, **Shubhranshu Bhandari:** Formal analysis, Investigation, Writing-review & editing, **Prabhakaran Selvaraj:** Data curation, **Senthilarasu Sundaram:** Supervision, Writing-review & editing, **Tapas K. Mallick:** Supervision, Project administration.

Declaration of Competing Interest

The authors declare that they have no known competing financial interests or personal relationships that could have influenced the work reported in this article.

Acknowledgement

The funding from Engineering and Physical Science Research Council through EUED Tech 2019 project (EP/S030786/1) is acknowledged. Besides, A.R. acknowledges the research Grant No. EP/T025875/1 received by Engineering and Physical Sciences Research Council (EPSRC), UK.

References

[1] K. P. Goetz, A. D. Taylor, Y. J. Hofstetter, Y. Vaynzof, Sustainability in perovskite solar cells, ACS Appl. Mater. Interfaces 13 (2021) 1. https://dx.doi.org/10.1021/acsami.0c17269

[2] M.-G. Ju, M. Chen, Y. Zhou, J. Dai, L. Ma, N. P. Padture, X.C. Zeng, Toward eco-friendly and stable perovskite materials for photovoltaics, Joule 2 (2018) 1231. https://doi.org/10.1016/j.joule.2018.04.026

[3] T. Wu, Z. Qin, Y. Wang, Y. Wu , W. Chen, S. Zhang, M. Cai, S. Dai, J. Zhang, J. Liu, Z. Zhou, X. Liu, H. Segawa, H. Tan, Q. Tang, J. Fang et. al., The main progress of perovskite solar cells in 2020-2021, Nano-Micro Lett. 13 (2021) 152, https://doi.org/10.1007/s40820-021-00672-w

[4] N.-G. Park, Research direction toward scalable, stable, and high efficiency perovskite solar cells, Adv. Energy Mater. 10 (2020) 1903106. https://doi.org/10.1002/aenm.201903106

[5] L. McGovern, M. H. Futscher, L. A. Muscarella, B. Ehrler, Understanding the stability of $MAPbBr_3$ versus $MAPbI_3$: suppression of methylammonium migration and reduction of halide migration, J. Phys. Chem. Lett. 11 (2020) 7127. https://dx.doi.org/10.1021/acs.jpclett.0c01822

[6] P. Su, Y. Liu, J. Zhang, C. Chen, B, Yang, C. Zhang, X. Zhao, **Pb**-based perovskite solar cells and the underlying pollution behind clean energy: dynamic leaching of toxic substances from discarded perovskite solar cells, J. Phys. Chem. Lett. 11 (2020) 2812. https://doi.org/10.1021/acs.jpclett.0c00503

[7] J. Li, J. Duan, X. Yang, Y. Duan, P. Yang, Q. Tang, Review on recent progress of lead-free halide perovskites in optoelectronic applications, Nano Energy 80 (2021) 105526. https://doi.org/10.1016/j.nanoen.2020.105526

[8] F. Hao, C.C. Stoumpos, D.H. Cao, R.P.H. Chang, M.G. Kanatzidis, Lead-free solid-state organic-inorganic halide perovskite solar cells, Nat. Photonics 8 (2014) 489. https://doi.org/10.1038/nphoton.2014.82.

[9] M. Wang, W. Wang, B. Ma et al. Lead-free perovskite materials for solar cells, Nano-Micro Lett. 13 (2021) 62. https://doi.org/10.1007/s40820-020-00578-z.

[10] M. Dhonde, K. Sahu, V.V.S. Murty, S.S. Nemala, P. Bhargava P. Surface plasmon resonance effect of Cu nanoparticles in a dye sensitized solar cell, Electrochim. Acta 249 (2017) 89. https://doi.org/10.1016/j.electacta.2017.07.187.

[11] X. Li, X. Zhong, Y. Hu, B. Li, Y. Sheng, Y. Zhang, Chao Weng, M. Feng, H. Han, J. Wang, Organic−inorganic copper(II)-based material: a low-toxic, highly stable light absorber for photovoltaic application, J. Phys. Chem. Lett. 8 (2017) 1804. https://doi.org/10.1021/acs.jpclett.7b00086.

[12] S.M. Menke, W.A. Luhman, R.J. Holmes RJ. Tailored exciton diffusion in organic photovoltaic cells for enhanced power conversion efficiency, Nat. Mater. 12 (2013) 152. https://doi.org/10.1038/nmat3467

[13] S. Uthayaraj, D.G.B.C. Karunarathne, G.R.A. Kumara, T. Murugathas, S. Rasalingam R.M.G. Rajapakse et al. Powder pressed cuprous iodide (CuI) as a hole transporting material for perovskite solar cells, Materials 12 (2019) 1. https://doi.org/10.3390/ma12132037

[14] D. Li, H. Ågren, G. Chen, Near infrared harvesting dye-sensitized solar cells enabled by rare-earth upconversion materials, Dalt Trans 47 (2018) 8526. https://doi.org/10.1039/c7dt04461e.

[15] Z. Song, Y. Jiang, J. Liu, Q. Pan, W. Zuo, X. Zhang et al. Copper incorporation in organic-inorganic hybrid halide perovskite solar cells, Chem. Select 3 (2018) 12198. https://doi.org/10.1002/slct.20180279

[16] J. Zhao, X. Zheng, Y. Deng, T. Li, Y. Shao, A. Gruverman et al. Is Cu a stable electrode material in hybrid perovskite solar cells for a 30-year lifetime? Energy Environ. Sci. 9 (2019) 3650. https://doi.org/10.1039/c6ee02980a

[17] G.A. Sepalage, S. Meyer, A. Pascoe, A.D. Scully, F. Huang, U. Bach et al. Copper(I) iodide as hole-conductor in planar perovskite solar cells: probing the origin of J-V hysteresis, Adv. Funct. Mater. 25 (2015) 5650. https://doi.org/10.1002/adfm.201502541.

[18] H.S. Shim, H.J. Kim, J.W. Kim, S.Y. Kim, W.I. Jeong, T. M. Kim et al. Enhancement of near-infrared absorption with high fill factor in lead phthalocyanine-based organic solar cells, J. Mater. Chem. 22 (2012) 9077. https://doi.org/10.1039/c2jm30417a.

[19] A.F. Holleman, E. Wiberg E (2001). Inorganic Chemistry. San Diego: Academic Press. ISBN 0-12-352651-5.

[20] J. Shamsi, A.S. Urban, M. Imran, L. De Trizio, L. Manna, Metal halide perovskite nanocrystals: synthesis, post-synthesis modifications, and their optical properties, Chem. Rev. 119 (2019) 3296. https://doi.org/10.1021/acs.chemrev.8b00644.

[21] A. Roy, H. Ullah, A. Ghosh, H. Baig, S. Sundaram, A. A. Tahir, T.K. Mallick, Understanding the semi-switchable thermochromic behavior of mixed halide hybrid perovskite nanorods, J. Phys. Chem. C 125 (2021) 18058. https://doi.org/10.1021/acs.jpcc.1c05487

[22] S. Bhandari S, A. Roy, A. Ghosh, T.K. Mallick, S. Sundaram, Performance of WO_3-incorporated carbon electrodes for ambient mesoscopic perovskite solar cells. ACS Omega 5 (2020) 422. https://doi.org/10.1021/acsomega.9b02934

[23] S. Bhandari S, A. Roy, A. Ghosh, T.K. Mallick, S. Sundaram, Perceiving the temperature coefficients of carbon-based perovskite solar cells, Sustainable Energy Fuels 4 (2020) 6283. https://doi.org/10.1039/D0SE00782J

[24] S. Luo, W. A. Daoud, Crystal structure formation of $CH_3NH_3PbI_{3-x}Cl_x$ perovskite, Materials 9 (2016) 123, https://doi.org/10.3390/ma9030123

[25] A. M. Elseman, A. E. Shalan, S. Sajid, M. M. Rashad, A. M. Hassan, M . Li, Copper-substituted lead perovskite materials constructed with different halides for working $(CH_3NH_3)_2CuX_4$-based perovskite solar cells from experimental and theoretical view, ACS Appl. Mater. Interfaces 10 (2018) 11699. https://doi.org/10.1021/acsami.8b00495

[26] M. Green, A. Ho-Baillie, H. Snaith, The emergence of perovskite solar cells. Nature Photon 8 (2014) 506. https://doi.org/10.1038/nphoton.2014.134

[27] Z. Shi, J. Guo, Y. Chen, Q. Li, Y. Pan, H. Zhang, Y. Xia, W. Huang, Lead-free organic-inorganic hybrid perovskites for photovoltaic applications: recent advances and perspectives, Adv. Mater. 29 (2017) 1605005, https://doi.org/10.1002/adma.201605005

[28] I. B. Ogunniranye, T. Atsue, O. E. Oyewande, Structural and optoelectronic behavior of the copper-doped $Cs_2AgInCl_6$ double perovskite: A density functional theory investigation, Phys. Rev. B 103 (2021) 024102. https://doi.org/10.1103/PhysRevB.103.024102

[29] Y. Shirahata, T. Oku, Photovoltaic properties of Cu-doped $CH_3NH_3PbI_3$ with perovskite structure. AIP Conf Proc 2017;1807. https://doi.org/10.1063/1.4974790.

[30] H. Tanaka, T. Oku, N. Ueoka, Structural stabilities of organic–inorganic perovskite crystals, Jpn. J. Appl. Phys. 57 (2018) 08RE12. https://doi.org/10.7567/JJAP.57.08RE12

[31] H. Rao, S. Ye, W. Sun, W. Yan, Y. Li, H. Peng, Z. Liu, Z. Bian, Y. Li, C. Huang, A 19.0% efficiency achieved in CuO_x-based inverted $CH_3NH_3PbI_{3-x}Cl_x$ solar cells by an effective Cl doping method, Nano Energy 27 (2016) 51–57. https://doi.org/10.1016/j.nanoen.2016.06.044

[32] X. Ge, X. Qu, L. He, Y. Sun, X. Guan, Z. Pang et al. 3D low toxicity Cu-Pb binary perovskite films and their photoluminescent/photovoltaic performance, J Mater. Chem. A 7 (2019) 27225. https://doi.org/10.1039/c9ta12736d

[33] S.R. Qiu, B.C. Wood, P.R. Ehrmann, S.G. Demos, P.E. Miller, K.I. Schaffers et al. Origins of optical absorption characteristics of Cu^{2+} complexes in aqueous solutions, Phys. Chem. Chem. Phys. 17 (2015) 18913. https://doi.org/10.1039/c5cp01688f.

[34] H. Takeda, Y. Monma, H. Sugiyama, H. Uekusa, O. Ishitani, Development of visible-light driven Cu(I) complex photosensitizers for photocatalytic CO_2 reduction, Front. Chem. 7 (2019) 418. https://doi.org/10.3389/fchem.2019.00418

[35] M. Ruthkosky, C. A. Kelly, F. N. Castellano, G. J. Meyer, Electron and energy transfer from Cu^I MLCT excited states, Coord. Chem. Rev. 171 (1998) 309. https://doi.org/10.1016/S0010-8545(98)90045-5

[36] Z. M. Gibbs, A. LaLonde, G. J. Snyde, Optical band gap and the Burstein–Moss effect in iodine doped PbTe using diffuse reflectance infrared Fourier transform spectroscopy, New J. Phys. 15 (2013) 075020. https://doi.org/10.1088/1367-2630/15/7/075020

[37] Q. Shen, Y. Ogomi, J. Chang, T. Toyoda, K. Fujiwara, K. Yoshino, K. Sato, K. Yamazaki et al., Optical absorption, charge separation and recombination dynamics in Sn/Pb

cocktail perovskite solar cells and their relationships to photovoltaic performances, J. Mater. Chem. A 3 (2015) 9308. https://doi.org/10.1039/C5TA01246E.

[38] W.-J. Chen, Y.-C. Lin, G. Kumar, S.-Y. Xie, F.-C. Chen, Polymer-capped copper nanoparticles trigger plasmonic field for improving performance of perovskite solar cells, Synthetic Metal 273 (2021) 116675. https://doi.org/10.1016/j.synthmet.2020.116675.

[39] X. Gen, M. Gu, An efficiency breakthrough in perovskite solar cells realized by Al-coated Cu nanoparticles, OSA Technical Digest (online) (Optical Society of America, 2016), paper JTh2A.145. https://doi.org/10.1364/FIO.2016.JTh2A.145

[40] F. Ünlü, E. Jung, J. Haddad, A. Kulkarni, S. Öz, H. Choi et al. Understanding the interplay of stability and efficiency in A-site engineered lead halide perovskites. APL Mater 8 (2020) 070901. https://doi.org/10.1063/5.0011851.

[41] Y. Wang, X. Liu, Z. Zhou, P. Ru, H. Chen, X. Yang, L. Han, reliable measurement of perovskite solar cells, Adv. Mater. 31 (2019) 1803231. https://doi.org/10.1002/adma.201803231

[42] C. Lu, W. Zhang, Z. Jiang, Y. Zhang, C. Ni, CuI/spiro-OMeTAD double-layer hole transport layer to improve photovoltaic performance of perovskite solar cells, Coatings 11 (2021) 978. https://doi.org/10.3390/coatings11080978

[43] M. M. Byrandvand, T. Kim, S. Song, G. Kang, S.U. Ryu, T. Park, p-Type CuI islands on TiO_2 electron transport layer for a highly efficient planar-perovskite solar cell with negligible hysteresis, Adv. Energy Mater. 8 (2018) 1702235, https://doi.org/10.1002/aenm.201702235**.**

[44] A. Swarnkar, W. J. Mir, R. Chakraborty, M. Jagadeeswararao, T. Sheikh, A. Nag, **Are** Chalcogenide perovskites an emerging class of semiconductors for optoelectronic properties and solar cell? Chem. Mater. 31 (2019) 565. https://doi.org/10.1021/acs.chemmater.8b04178

[45] M. Pazoki, T. Edvinnson, Metal replacement in perovskite solar cell materials: chemical bonding effects and optoelectronic properties, Sustainable Energy Fuels 2 (2018) 1430. https://doi.org/10.1039/C8SE00143J

[46] A. Liu, H. Zhu, M.-G. Kim, J. Kim, Y.-Y. Noh, Engineering copper iodide (CuI) for multifunctional p-Type transparent semiconductors and conductors, Adv. Sci. 8 (2021) 2100546. https://doi.org/10.1002/advs.202100546

[47] K. Ahmed, S. M. Mobin, Organic–inorganic copper (II)-based perovskites: a benign approach toward low-toxicity and water-stable light absorbers for photovoltaic applications, Energy Technol. 8 (2020) 1901185. https://doi.org/10.1002/ente.201901185

[48] S. Yeu, K. Liu, R. Xu, M. Li, M. Azam, K. Ren, J. Liu, Y. Sun, Z. Wang, D. Cao et al., Efficacious engineering on charge extraction for realizing highly efficient perovskite solar cells, Energy Environ. Sci. 10 (2017) 2570. https://doi.org/10.1039/C7EE02685D

[49] E. Horváth, M. Kollár, P. Andričevic, L. Rossi, X. Mettan, L. Forró L. Fighting health hazards in lead halide perovskite optoelectronic devices with transparent phosphate salts, ACS Appl. Mater. Interfaces 13 (2021) 33995. https://doi.org/10.1021/acsami.0c21137.

[50] Z. Xiao, K.-Z. Du, W. Meng, D.B. Mitzi, Y. Yan, Chemical origin of the stability difference between copper(I)- and silver(I)-based halide double perovskites, Angew.Chem. Int.Ed. 56 (2017) 12107 –12111. https://doi.org/10.1002/anie.201705113

[51] B. A. Connor, R. W. Smaha, J. Li, A. Gold-Parker, A. J. Heyer, M. F. Toney, Y. S. Lee, H. I. Karunadasa, Alloying a single and a double perovskite: a $Cu^{+/2+}$ mixed-valence layered halide perovskite with strong optical absorption, Chem. Sci. 12 (2021) 8689-8697. https://doi.org/10.1039/D1SC01159F

[52] L.-Y. Bi, T.-L. Hu, M.-Q. Li, B.-K. Ling, M. S. Lassoued, Y.-Q. Hu, Template effects in Cu(I)-Bi(III) iodide double perovskites: a study of crystal structure, film orientation, band gap and photocurrent response, J. Mater. Chem. A 8 (2020) 7288-7296. https://doi.org/10.1039/D0TA00949K

[53] X. Li, F. Zhang, H. He, J. J. Berry, K. Zhu, T. Xu, On-device lead sequestration for perovskite solar cells. Nature 578 (2020) 555. https://doi.org/10.1038/s41586-020-2001-x.